Lab on a Chip

PAPER

View Article Online
View Journal | View Issue

Open Access Article. Published on 18 May 2015. Downloaded on 7/17/2025 8:03:40 PM.
This article is licensed under a Creative Commons Attribution-NonCommercial 3.0 Unported Licence.

Cite this: *Lab Chip*, 2015, **15**, 2981

Tailoring three-dimensional architectures by rolled-up nanotechnology for mimicking microvasculatures

Rerngchai Arayanarakool,*[a] Anne K. Meyer,[a] Linda Helbig,[a] Samuel Sanchez[bcd] and Oliver G. Schmidt[ae]

Received 7th January 2015,
Accepted 16th May 2015

DOI: 10.1039/c5lc00024f

www.rsc.org/loc

Artificial microvasculature, particularly as part of the blood–brain barrier, has a high benefit for pharmacological drug discovery and uptake regulation. We demonstrate the fabrication of tubular structures with patterns of holes, which are capable of mimicking microvasculatures. By using photolithography, the dimensions of the cylindrical scaffolds can be precisely tuned as well as the alignment and size of holes. Overlapping holes can be tailored to create diverse three-dimensional configurations, for example, periodic nanoscaled apertures. The porous tubes, which can be made from diverse materials for differential functionalization, are biocompatible and can be modified to be biodegradable in the culture medium. As a proof of concept, endothelial cells (ECs) as well as astrocytes were cultured on these scaffolds. They form monolayers along the scaffolds, are guided by the array of holes and express tight junctions. Nanoscaled filaments of cells on these scaffolds were visualized by scanning electron microscopy (SEM). This work provides the basic concept mainly for an *in vitro* model of microvasculature which could also be possibly implanted *in vivo* due to its biodegradability.

Introduction

In microvascular engineering, the scaffold for mimicking blood vessels plays an essential role in cell responses, *e.g.*, cell differentiation, cell alignment, cell elongation, gene expression, and tight-junction formation.[1–9] Therefore, a cylindrical structure resembling the shape of a blood vessel is a more rational approach to mimic vascular microenvironment rather than conventional rectangular ones made from microfluidic channels for *in vitro* studies.[10–19] As a scaffold for cell culture, the tubular structure should comprise access to nutrients. With nanotechnology methods, well-defined micro- and nanostructures can be precisely fabricated to create two-dimensional (2D) architectures for exploitation in diverse fields of life science and engineering. Recently, three-dimensional (3D) architectures have gained more popularity since they resemble physiological microenvironments more closely.[20–24] For bilayer cell culture, scaffolds should provide physical support while allowing direct contact of both cells in and outside the tube. In this way, cells can create tight junctions in order to perform a biological barrier function. In general, cell–cell communication is dependent on direct physical contact or indirect contact *via* soluble factor regulation.[21,22,25]

Lumen formation of endothelial cells (ECs) in 3D scaffolds of hydrogels[26–30] which are able to be engineered as a vascular extracellular matrix[31] has been demonstrated as an excellent system to mimic vasculature especially for *in vivo* applications. However, in order to mimic vasculature from arteries to capillaries, a tubular structure with a diameter down to 10 μm (*e.g.*, a capillary in the brain) should be chosen. Hydrogels are fluids and do not offer stability or variability in size during lumen formation, and porous cylindrical structures for cell culture have not reached diameters below 100 μm.[32] Additionally, in hydrogels, vessel-like structures form spontaneously and not in a directed or designed fashion. Importantly, in hydrogel-based devices, cells embedded in 3D matrices obstruct the employment of imaging methods which are critical to nanoscale analysis. Contrarily, cells populating porous tubes can be visualized by SEM and confocal analysis with low background noise from scaffolds. Thus, the scalable, porous and tubular scaffold should provide a good platform for mimicking a microvasculature system especially for *in vitro* applications. Such a system would have advantages for drug science due to its controllability in miniaturized dimensions (tiny holes and small tube diameter), functionalization, reproducibility, and high-resolution optical imaging.

[a] *Institute for Integrative Nanosciences, Leibniz Institute for Solid State and Materials Research Dresden, Helmholtzstraße 20, 01069, Dresden, Germany. E-mail: rerngchaia@yahoo.com*
[b] *Max Planck Institute for Intelligent Systems, Heisenbergstraße 3, 70569 Stuttgart, Germany*
[c] *Institut de Bioenginyeria de Catalunya (IBEC), Baldiri i Reixac 10-12, 08028 Barcelona, Spain*
[d] *Institució Catalana de Recerca i Estudis Avancats (ICREA), Pg. Lluís Companys 23, 08010, Barcelona, Spain*
[e] *Materials Systems for Nanoelectronics, TU Chemnitz, 09107, Chemnitz, Germany*

Open Access Article. Published on 18 May 2015. Downloaded on 7/17/2025 8:03:40 PM.
This article is licensed under a Creative Commons Attribution-NonCommercial 3.0 Unported Licence.

Three-dimensional architectures fabricated by strain engineering technologies[33,34] were first reported as a platform for cell culture by Mei and Huang *et al.*[35,36] and established as a "lab-in-a-tube" application[37] for investigating neuronal guidance, cell mobility and cell division inside confined space.[38–43] In order to create uniform, continuous porous tubes for cell layer formation, we here advance our fabrication approach to roll up nanomembranes with specified arrays of holes. In our approach, the diameter and number of windings can be controlled by the geometry of the thin film. Strain-engineered scaffolds with access holes and metallic patterns were reported before by Jamal *et al.*,[44] and our work here shows scalability of tube diameter down to 10 μm for capillaries, tunability of access holes for direct or non-direct contact of cells, tiny holes and tube curvature for homogeneous cell adhesion, and biodegradability of scaffolds. Another important aspect of our work is the use of ECs as a specific cell type forming endothelial boundaries potentially allowing for the future use as drug-testing platforms and gaining the possibility of evaluating speed and efficiency of drug passing through vessels (*i.e.*, blood–brain boundary). Although this work mainly focus on the scaffolds as an *in vitro* model of microvasculature, the biodegradability of this three-dimensional structure is also demonstrated for the future use as an *in vivo* implant.

We demonstrate the fabrication and employment of this tubular microstructure as a cell scaffold to mimic microvasculature by culturing ECs or astrocytes around the scaffolds. ECs populate porous tubes and form a monolayer with tight junctions. Astrocytes are specifically guided to those parts of the tubes that contain holes. We fabricated metal patterns inside porous tubes offering the opportunity for specific functionalization areas or integration of a sensing system inside porous tubes. The fabrication approach of this cell scaffold was adjusted to enable the biodegradability in culture medium. This allows cells to form a monolayer or a bilayer where the mechanical support dissolves after layer formation. These porous tubes are capable of being integrated into microfluidic systems or rolled-up electrodes, offering the opportunity to build cylindrical-shaped microvasculature networks or to perform real-time electrical measurement on a miniaturized device.[45,46]

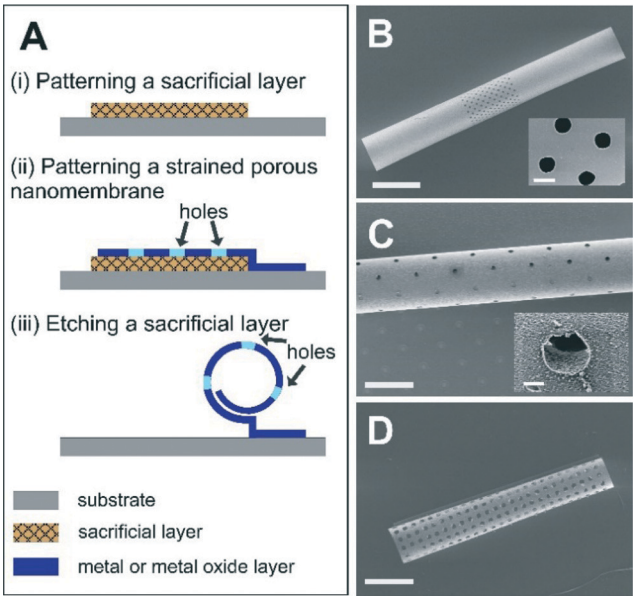

Fig. 1 (A) Schematic of the fabrication procedure of porous tubes. (B–D) SEM image of a porous tube was fabricated by rolling up a porous strained membrane (SiO and SiO_2 layers). (B) The tube contains an array of holes in the middle with a tube diameter of 70 μm and a hole diameter of 4 μm (inset). (C) The tube (20 μm in diameter) contains holes of 2 μm (inset). (D) The holes are rectangular-shaped with the pattern of holes along the entire tube with a tube diameter of 18 μm. The scale bars are 100 (B), 5 (inset of B), 20 (C and D) and 1 μm (inset of C), respectively.

Materials and methods

Rolled-up porous tube fabrication

The porous tubes were fabricated by employing the rolled-up technology and standard photolithography as illustrated in Fig. 1A. First, a glass substrate was cleaned with organic solvents (acetone and isopropanol, respectively) and dried by nitrogen before dehydration at 120 °C for 5 min. A sacrificial layer was then patterned onto this substrate by using a lift-off process. This process was started by spin-coating a negative photoresist (AZ5214E, Clariant GmbH) onto this substrate (4500 rpm, 30 s) and patterned by a mask aligner (MJB4, SÜSS Microtec). Subsequently, a metallic sacrificial layer was deposited onto this substrate with a patterned photoresist by using electron beam evaporation (Edwards AUTO 500 E-beam evaporator) under high vacuum ($<10^{-4}$ Pa). Afterwards, the sample was cleaned with organic solvent to remove the photoresist. Then, the second lift-off process was performed by using the same procedure as described above to create the pattern of strained nanomembrane with the array of holes by E-beam deposition prior to removing the photoresist with organic solvent. In our experiment, we used copper (40 nm thick) as a sacrificial layer which can be removed with a chromium etching solution (Chromium Etch no.1, Microchem) within a few minutes. Upon the etching step, the nanomembrane with the array of holes started to roll up due to the mismatched strains of bimetallic or oxide layers forming a rolled-up porous tube.[33,34] Finally, the sample was rinsed with DI water for a few minutes before drying in a critical point dryer (CPD 030, Bal-Tec AG) to avoid the structural collapse. The microtube was further coated with a 15 nm Al_2O_3 layer by using atomic layer deposition (ALD, SavannahTM 100, Cambridge NanoTech Inc.) to strengthen the microtubes. All organic solvents were purchased from VWR GmbH.

Characterization

The micro- and nanostructures of microtubes were imaged by using an optical microscope (Zeiss Axiocam MR) and a

 This journal is © The Royal Society of Chemistry 2015

Open Access Article. Published on 18 May 2015. Downloaded on 7/17/2025 8:03:40 PM.
This article is licensed under a Creative Commons Attribution-NonCommercial 3.0 Unported Licence.

SEM (Zeiss Digital) with 1–5 keV acceleration voltage. Before imaging, the samples were coated with 5 nm gold.

Biofunctionalization of porous tube

After being fabricated by the aforementioned approach, the porous tube was functionalized to promote good adhesion of cells along the scaffold. First, the tube was cleaned with oxygen plasma (30 W, 5 min) and then immersed in 1 mM 11-phosphonoundecanoic acid in toluene overnight. Afterwards, it was thoroughly rinsed with toluene, acetone, ethanol and water, respectively, and dried by nitrogen. Then it was immersed in PBS solution containing 0.1 M *N*-(3-dimethylaminopropyl)-*N*-ethylcarbodiimide (EDC) and 0.025 M *N*-hydroxyl sulfosuccinimide (NHS) (1 hour) followed by incubation with 0.02 mg mL^{-1} fibronectin at 37 °C (1 hour). Then, the sample was immersed in EDC and NHS for one hour. In order to improve *in vitro* microvasculature, the porous tube was further coated by collagen matrices (collagen type I, Gibco) to imitate the mechanical properties of this scaffold to soft tissue by following the protocol from the manufacturer. Firstly, collagen (5 mg mL^{-1}) was mixed with sterile 10× PBS, sterile distilled water and sterile 1 M NaOH to obtain the final collagen concentration of 3 mg mL^{-1} at pH 7. Then, the collagen solution was immediately dispensed into the microtube array and incubated at 37 °C in a humidified incubator (30 min). Finally, the samples were rinsed with sterile PBS before seeding cells. All chemicals were purchased from Sigma Aldrich.

Cell culture

The porous tubes were used as scaffolds to culture two cell lines, *i.e.*, endothelial cells (b.End3) and astrocytes (C8D1A) purchased from ATCC. Cells were cultured in cell medium (Dulbecco's modified Eagle's medium (DMEM), Sigma Aldrich), 10% fetal bovine serum (FBS, Sigma Aldrich), 2 mM L-glutamine (Sigma Aldrich), 1% penicillin/streptomycin (Gibco) at 37 °C in a humidified atmosphere containing 5% CO_2. Cells were placed onto the microporous tube array at a concentration of 5×10^4 cells per mL and cultured for 2–3 weeks. The medium was refreshed every 2–3 days. Vascular endothelial growth factor (VEGF, 10 ng mL^{-1}, PAN Biotec) was added to the endothelial cells to improve vascularisation.

Immunostaining and fluorescence imaging

The cell culture samples for fluorescence imaging were fixed in cold ethanol at −20 °C for 10 min and then rinsed three times with PBS solution. The samples were subsequently permeabilized in 0.1% Triton X-100/PBS (10 min) at room temperature. Afterwards, they were blocked in 1% bovine serum albumin (BSA) in PBS for 1 h. Then, the cell samples were incubated with primary antibody (monoclonal mouse anti-ZO-1 antibody, 10 μg mL^{-1}; Invitrogen) diluted in 1% BSA/PBS overnight at 4 °C to label ZO-1 protein. Secondary antibodies coupled to Alexa Fluor 594 goat anti-mouse (Invitrogen) were used at 1 : 500, phalloidin–FITC (Invitrogen) at 1 : 160 was used to label actin filaments, and DNA was stained using 4, 6-diamidino-2-phenylindole (DAPI, Invitrogen) in PBS for 1 hour incubation at room temperature. Then, the samples were rinsed in PBS three times. Finally, the cell culture samples were placed between two glass coverslips prior to imaging by using an inverted fluorescence microscope (AxioObserver Z1, Zeiss) or a Zeiss LSM 780 confocal microscope.

SEM imaging of cell culture samples

The preparation of cell culture samples for SEM imaging was done by following the protocol published before.[47] Briefly, the samples were incubated in 3% glutaraldehyde (Sigma-Aldrich) in 0.1 M PBS at 37 °C (15 min) and then rinsed three times with PBS solution. Subsequently, they were treated in 1% osmium tetraoxide (Roth) in PBS at pH 7.4 (30 min) and then rinsed in PBS solution five times. After incubation in 1% carbohydrazide (30 min), the samples were rinsed five times in DI water (15 min). They were then incubated again in osmium tetraoxide solution (30 min) before rinsing thoroughly with DI water (15 min). The samples were then dehydrated through ethanol solution series from 30%, 50%, 70%, 90% and (three times) 100% ethanol solution over 30 min. Finally, they were dried in critical point dryer and coated with 5 nm gold.

Biodegradation of SiO and SiO_2 layers

The thin films (90 nm) of SiO or SiO_2 which were prepared by E-beam evaporation were immersed in the culture medium and placed in an incubator at 37 °C. After specific periods of time, they were thoroughly rinsed with water and dried under nitrogen flow prior to the measurement of the thickness using a profilometer. The biodegradation of this porous tube was done by culturing ECs in culture medium for 5 weeks.

Results and discussion

Porous tubes with diverse geometries and materials

Microtubular structures with arrays of holes can be fabricated as shown in Fig. 1A. The length of porous tubes and the patterns of holes are designed and scaled down to the resolution limit of a standard photolithography. For instance, holes can be 4 μm (Fig. 1B) or 2 μm (Fig. 1C) in diameter. Different patterns of holes are shown in Fig. 1B (middle of a tube) and D (entire tube), and the different shapes of holes are shown in Fig. 1B (circular shape) and D (rectangular shape). The diameter of the tubes was tuned by altering thicknesses and deposition rates of materials to employ them as scaffolds for vascularisation at different vessel diameters (Fig. 2). Physical vapour deposition allowed utilising different materials for fabrication of porous tubes (Fig. 3). Importantly, one porous tube can incorporate different materials yielding diverse functionalization. For example, a gold surface inside a tube can be used for thiol functionalization and a SiO_2 surface outside a tube for silanization. Moreover, it is possible to make micro-metallic patterns (Fig. 3J and K) allowing for

Open Access Article. Published on 18 May 2015. Downloaded on 7/17/2025 8:03:40 PM.
This article is licensed under a Creative Commons Attribution-NonCommercial 3.0 Unported Licence.

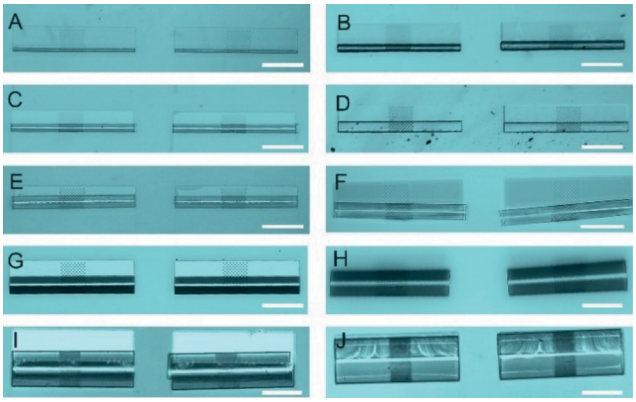

Fig. 2 The diameters of porous tubes can be tuned by altering the thickness or the deposition rate during nanomembrane production. The tubes consist of an array of holes only in the middle part with a hole diameter of 2–4 μm and an array length of around 120 μm. Porous tubes were made from SiO/SiO_2 membranes (A–F and J), SiO_2/TiO_2 membrane (G, H) and TiO_2 membrane (I). The tube diameters were approximately 15 (A), 30 (B), 40 (C), 50 (D), 60 (E), 70 (F), 80 (G), 125 (H), 170 (I) and 225 μm (J). The scale bars for all images are 200 μm.

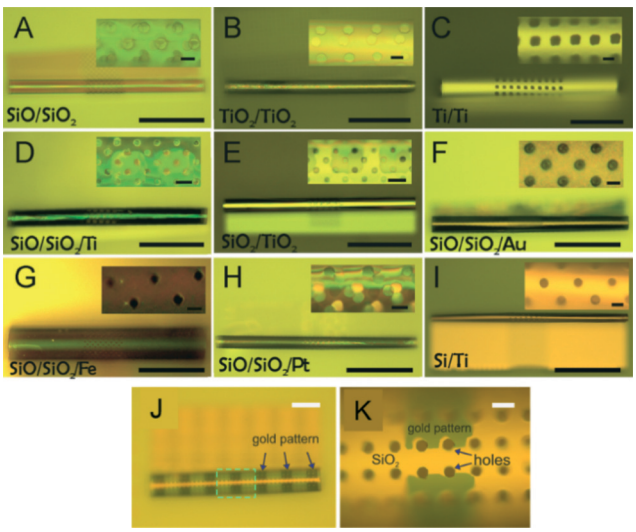

Fig. 3 Porous tubes can be made from different materials providing versatile functionality. The tubes were made from SiO/SiO_2 (A), TiO_2/TiO_2 (B), Ti/Ti (C), $SiO/SiO_2/Ti$ (D), SiO/TiO_2 (E), $SiO/SiO_2/Au$ (F), $SiO/SiO_2/Fe$ (G), $SiO/SiO_2/Pt$ (H), and Si/Ti (I). (J) Porous tubes with an integrated gold pattern. (K) Magnified image of the middle part of a SiO_2 tube with a hole diameter of 4 μm and gold patterns. Gold patterns can be used for localized functionalization such as sensing inside a tubular structure. The scale bars for all images are 200 μm, except for C, J, and K, which are 15, 100, and 10 μm, respectively. The insets are the magnified images of the hole array in the middle area of each porous tube. The scale bars for all insets are 5 μm except for the inset of C, which is 2 μm.

spatial functionalization or real-time and vicinity sensing inside a tube.[46]

After rolling up, a short membrane created a porous tube with a few (<2) windings (Fig. 4A) providing pass-through holes. Such tubes were suitable for exploring direct physical contact between cells inside a tube and cells outside a tube. On the other hand, long membranes created a porous tube with several (>2) windings so that the holes in each layer did not overlap with those of neighboring layers (Fig. 4B and C), which could be useful for investigations of indirect communication between cells. In this case, cells cannot establish direct cell-to-cell contact because the apertures are too small for cell filament to pass. In this way, communication between cells in and outside of a tube can only rely on indirect soluble factor communication.[21] The dimensions of holes were downscaled with our fabrication approach to 2 μm which is the limit of standard photolithography. Overlapping holes create diverse periodic 3D configurations, for example, miniaturized apertures around the overlapping holes resulted in periodic star-shaped patterns (Fig. 4E and H) and I-shaped patterns (Fig. 4F and I). These 3D architectures were dependent on the patterns of holes, the dimensions of nanomembranes before rolling, and the diameter of the tubes which were all controllable in our approach.

Cell culture around porous tubes

After culturing cells around the porous tubes, we studied the cell morphology and cellular components by immunostaining. In the culture system of astrocytes on porous tubes, astrocytes grew around tubes and migrated into tubes particularly to the patterns of holes (Fig. 5). A single confocal image at the bottom of a tube (Fig. 5A) demonstrated that cells migrated into tubes and rather adhered to the part of the tube where holes are present. In this area, in tubes with

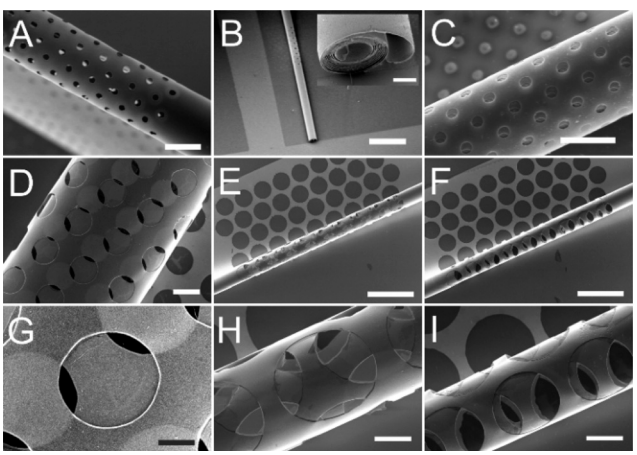

Fig. 4 Diverse configurations of the 3D architectures formed by rolling up a nanomembrane with hole patterns. (A) A porous tube with one winding is fabricated from a short porous membrane providing tiny pass-through holes. (B) The porous tube with several windings (B inset) is fabricated from the long membrane without pass-through holes (C) allowing only tiny objects or molecules to pass through. Nanoscaled periodic hole patterns can be made from the overlapped holes of this structure (D–I). Magnified images of periodic patterns in D, E, and F are shown in G, H and I, respectively. For instance, the dimension of the original hole pattern is 4 μm, and after rolling up, the overlapped holes create smaller aperture with dimensions of 0.5 μm by 2 μm (D and G). The scale bars are 20 μm (A), 100 μm (B), 5 μm (inset of B), 10 μm (C), 5 μm (D), 50 μm (E and F), 2 μm (G), and 10 μm (H and I).

 This journal is © The Royal Society of Chemistry 2015

Open Access Article. Published on 18 May 2015. Downloaded on 7/17/2025 8:03:40 PM.
This article is licensed under a Creative Commons Attribution-NonCommercial 3.0 Unported Licence.

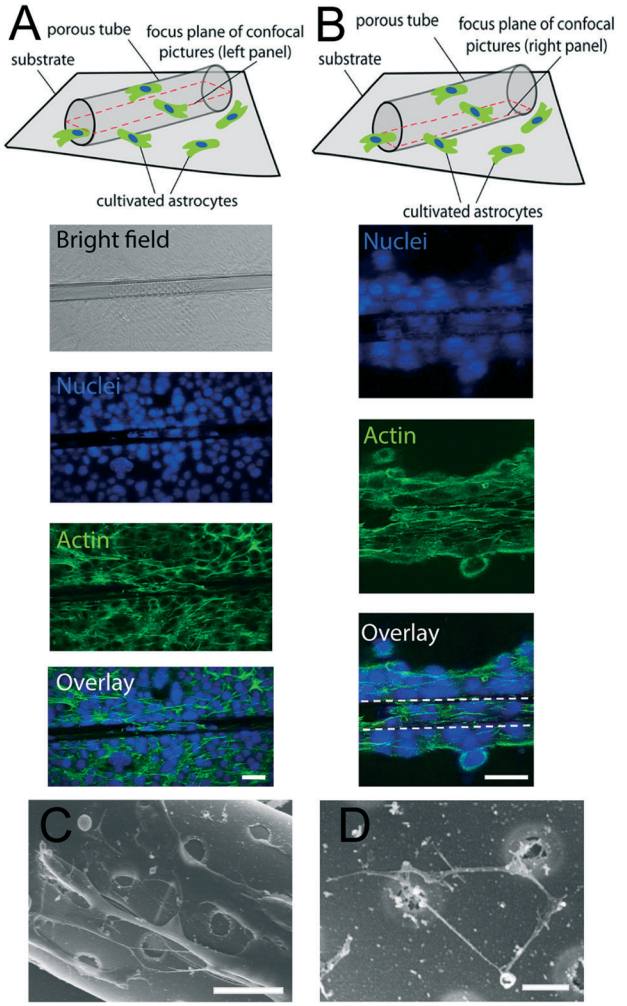

Fig. 5 Confocal images of astrocytes around a porous tube. (A) Confocal image taken at the bottom of the sample (*z*-position of the image slice illustrated above). (B) Confocal image in the middle of the sample (in *z*-direction as illustrated above). (C) SEM images of astrocytes seeded around the porous tube. (D) High-resolution of SEM allowed visualization of nanoscaled cellular components around porous tubes. The scale bars are 50 (A, B), 10 (C) and 2 μm (D), respectively.

<2 windings, cells can directly contact cells outside of the tube through holes allowing direct contact communication. A single confocal image in the middle plane of a tube showed that astrocytes were also able to climb the walls of the tubes (Fig. 5B), leading to a layer of astrocytes around the circumference of the tube. In scanning electron microscopy images, filaments that spread along the tubes as well as sprouting from the inside to the outside of tubes with <2 windings that allow direct passing through holes were visible (Fig. 5C and D). This emphasized that the connectivity of cells inside and outside of porous tubes is changing with the amount of windings. The porous tube with few windings allowing direct contact and communication between cells, while many windings prevent cell filaments to reach from one side to the other, this way allowing only indirect communication between cells, while the tube with many windings prevent cell filaments to reach from one side to the other, this way allowing only indirect communication *via* soluble factors.

Recently, researchers have promoted the growth and adhesion of ECs and lumen formation by replicating the substrate stiffness of soft tissue and/or adding vascular endothelial growth factor (VEGF).[48,49] Therefore, we further investigated the influence of coating with extracellular matrices such as collagen and adding VEGF (Fig. 6). 3D reconstruction of confocal stacks revealed ECs occupying the outer walls of porous tubes (Fig. 6A) with or without addition of VEGF and/or collagen to the samples. When VEGF was added, more cells climbed the walls of tubes and formed tighter monolayers, as shown by the expression of ZO-1 at the cell membranes (Fig. 6B and C). ZO-1 is a protein forming highly specialized epithelial junctions in endothelial cells. These tight junctions form a diffusion barrier to control the transport of molecules through the cell monolayer which is a hallmark of an endothelial cell layer. Importantly, tight junctions were not only formed in between cells (Fig. 6B) but also between cells and porous tubes (Fig. 6C). When VEGF and collagen were added to the samples, on top of the porous tubes, the cells formed a tight monolayer, as shown by tight junctions between all cells in that *z*-plane (Fig. 6D). Across the lateral walls of the porous tubes, ECs were able to form an endothelial bilayer. This means that one layer of cells formed on the inside of the wall and the other layer on the outside of the same wall, creating a bilayer on two sides of an integrated nanomembrane (Fig. 6E). When collagen was used to enhance the elasticity of the sample, more lumen formation was observed. These lumina frequently spanned from the flat surface toward patterns of holes on porous tubes (Fig. 6F). The combination of VEGF and collagen on porous tube substrates was most successful in inducing vascularization from porous tubes (Fig. 6G).

By using porous tubes, monolayer formation of ECs became possible for different diameters (Fig. 7). This allowed mimicking of different sizes of vasculature from arteries to capillaries. In summary, porous tubes supported the production of endothelial monolayers that are capable of performing a biological barrier function, as well as bilayers and lumen formation of ECs.

Biodegradation of porous tubes

It was reported before that thin layers of silicon oxides (SiO and SiO_2) dissolve in the buffer solution.[50] In our regular experiments, the porous tubes were made of SiO and SiO_2 and later coated with Al_2O_3 using atomic layer deposition to stabilise the SiO/SiO_2 scaffold. Tubes coated with alumina were stable for more than 6 weeks in culture medium since alumina prevented dissolution of silicon oxides.[51] However, in the absence of alumina, silicon oxide layers dissolved in cell culture medium. The thin layer of these oxide membranes dissolved in the medium at a rate of around 10 nm day^{-1} (Fig. 8A). We also investigated the biodegradability of

Open Access Article. Published on 18 May 2015. Downloaded on 7/17/2025 8:03:40 PM.
This article is licensed under a Creative Commons Attribution-NonCommercial 3.0 Unported Licence.

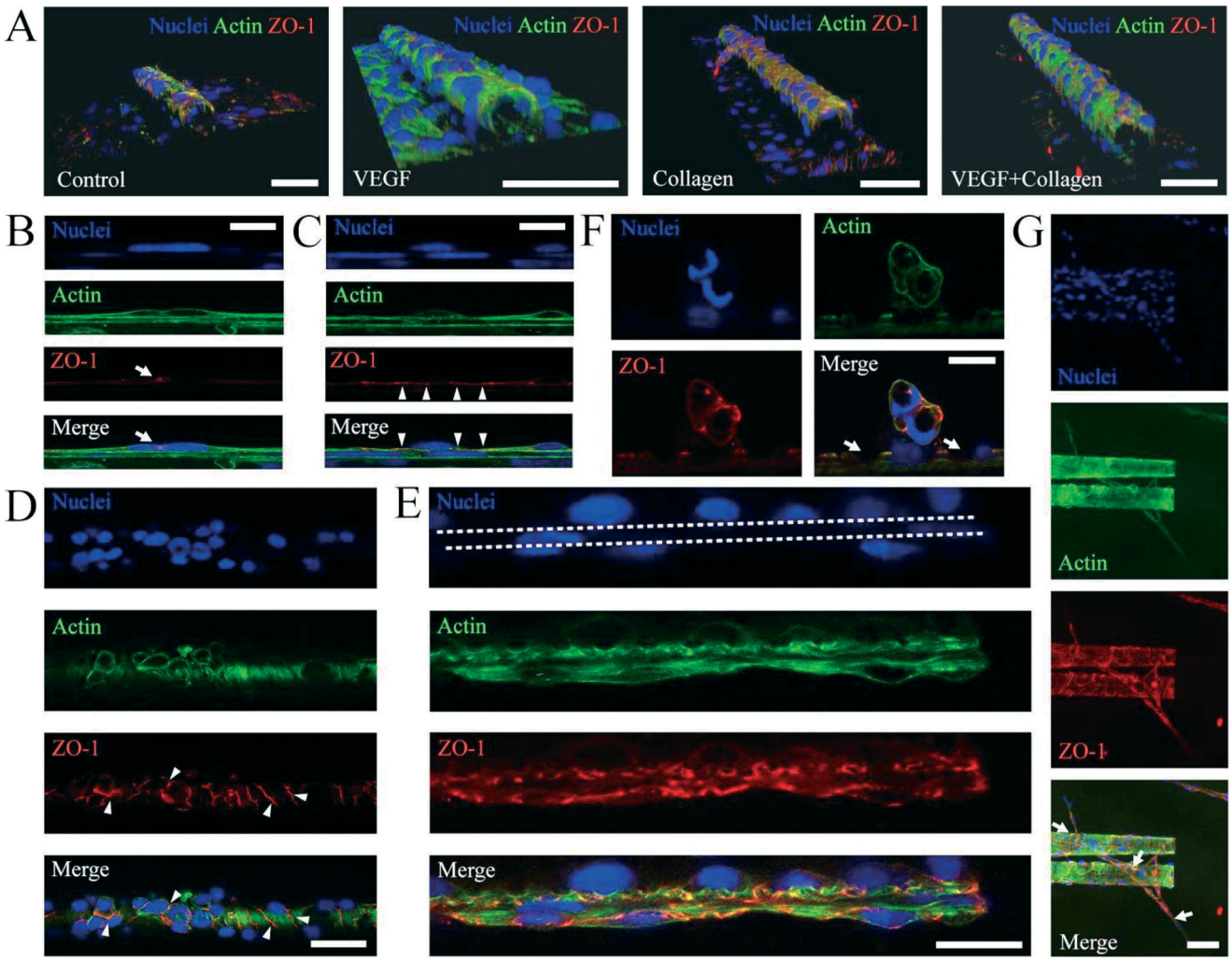

Fig. 6 Confocal images of endothelial cells seeded on porous tubes. (A) 3D reconstructions from confocal stacks. The scale bar is 50 μm. (B, C) Tight junctions between cells (arrows, B) and between cells and porous tubes (arrowheads, C). The scale bars are 10 μm. (D) Tight junctions between cells (arrowheads) on top of the tube. The scale bar is 20 μm. (E) Endothelial bilayer formation on two sides (in and out) of the lateral tube wall. The scale bar is 10 μm. (F) Lumen formation attached to the holes of the tube (arrows). The scale bar is 10 μm. (G) Multiple lumina form on the double tubes and connect them to the flat surface. The scale bar is 50 μm.

porous tubes in contact with EC culture. The rolled-up porous tubes which were made of SiO and SiO_2 (40 and 175 nm in thickness, respectively) and functionalized with collagen (without alumina coating) were used as scaffolds to culture ECs. The tube consisted of 4 windings of SiO/SiO_2 layers with the total wall thickness of around 860 nm. Cells formed a monolayer around the tube and became confluent in 2–3 weeks. They formed lumina from several positions, both on the flat substrate and around the tube as indicated by numbers 1, 2 and 3 in Fig. 8B–D. The tubes which were covered by ECs started bending from the middle part after 24 days of culture (Fig. 8B and C) and eventually deformed their shape after 33 days (Fig. 8D). The bending of tubes was due to the contraction force from the lumina which were connecting a tube to the flat area of the sample as indicated by numbers 1, 2 and 3 in Fig. 8B–D. The dissolution of thin films and deformation of porous tubes confirmed the biodegradation of these materials in culture medium. In summary, we have shown a versatile approach to fabricate tunable porous tubes for biological layer formation of ECs which can be biodegradable,

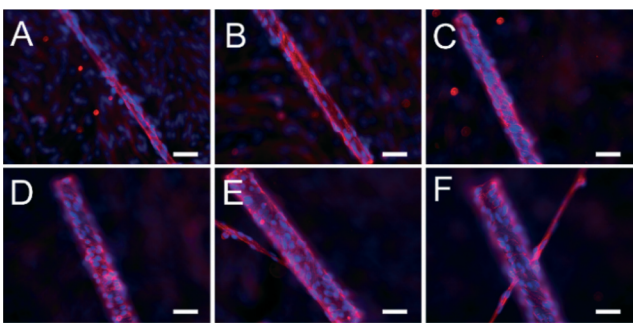

Fig. 7 The formation of EC monolayer at different diameters, *i.e.*, 12 (A), 20 (B), 30 (C), 40 (D), 50 (E), and 60 μm (F). The blue channel is the nucleus, and the red channel is ZO-1. The scale bars for all images are 50 μm.

 This journal is © The Royal Society of Chemistry 2015

Open Access Article. Published on 18 May 2015. Downloaded on 7/17/2025 8:03:40 PM.
This article is licensed under a Creative Commons Attribution-NonCommercial 3.0 Unported Licence.

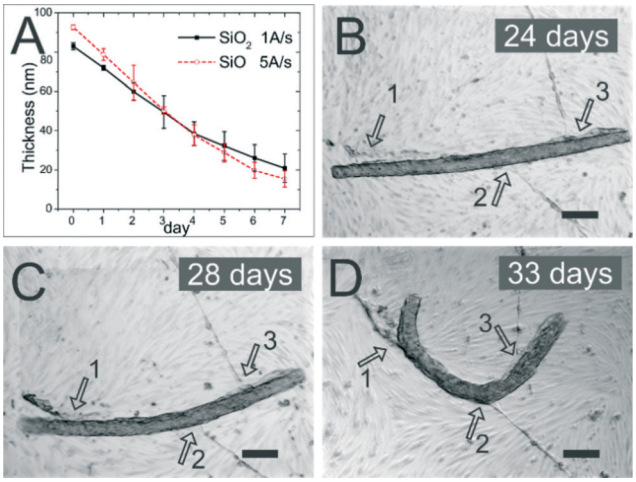

Fig. 8 (A) The dissolution of the SiO layer (dashed line) and SiO_2 layer (solid line) in culture medium. SiO and SiO_2 were deposited by using E-beam evaporation with a rate of 5 and 1 Å s^{-1}, respectively. The dissolution rate in culture medium (pH 7.4) is around 10 nm day^{-1} for both layers. (B–D) The collagen-coated porous tube which was seeded by ECs was deformed in culture medium for a few weeks. ECs formed lumens on the flat surface and around the tube as indicated by numbers 1, 2 and 3. At the 24th day, the porous tube started to bend from the middle. At the 33rd day, the tube deformed their shape in several positions. The scale bars are 100 μm.

functionalized and integrated into lab-in-a-tube devices for drug discovery.

Discussion

Our versatile fabrication approach can reproducibly generate high-throughput porous tubular structures with scalable sizes of pores and tube diameters to mimic microvasculature as the size of the pores is defined by photolithography and the tube diameter is dependent on the thicknesses and deposition rates of the nanomembrane materials as depicted in Fig. 2–4. These structures offer cylindrical shape, apertures around the tube, and the possibility of micropatterning inside porous tubes. Guidance of astrocytes and lumen formation of ECs demonstrated the proof-of-principle for the application as artificial microvasculature. Additionally, porous tubes with varied numbers of windings and diverse sizes of holes can be used for investigations of different cell–cell communication pathways. We here used tubular structures with holes to study the formation of biological barriers that require physical contact of cells. However, porous tubes can also be fabricated with several windings without pass-through holes for the investigation of indirect communication of cells. There, porous tubes act as a barrier to inhibit direct cell contact, while small molecules can pass through space between windings and non-overlapping holes. It was reported that ECs directly in contact with astrocytes *via* 3 μm holes exhibited heterogeneous behaviours compared to those cells which were indirectly contacted *via* sub-micron holes,[25] emphasizing the significant role of barrier for cell–cell communication. This will be the specific design criteria to make the cylindrically-shaped tubular scaffold suitable for investigation of cell responses in the EC/astrocyte co-culture system. Apart from this, the diameter of the tubular structure should be large enough for cells migrating inside. In addition, biodegradability enables porous tubes to stabilize lumen formation of desirable dimensions and to dissolve after formation is complete.

Outlook

Different functionalizations or real-time and vicinity sensing inside a tube[46] can be made inside our tubular structure which is difficult to perform in polymer-based devices.[27,52–54] For example, one can measure nitric oxide released from ECs intrinsically to link biological functions of blood vessels, *i.e.*, vascular muscle relaxation,[55–57] or monitor simultaneously the confluence and development of tight junctions of ECs by measuring trans-endothelial electrical resistance (TEER).[20] In this work, we use copper as a sacrificial layer requiring the etching solution of perchloric acid and ammonium cerium nitrate which is hazardous for cells. However, in the future, one can try to use PBS solution to etch copper[58] or change to water-soluble polymers.[59] This would allow us to roll up seeded cells together with the nanomembrane in PBS or water solution. Moreover, fabrication of microtubes on a substrate surface provides the opportunity to employ this structure for the field of body on a chip which was recently established.[60–63] This compartmented system will be useful as a co-culture system of microvasculature of ECs and other biological systems outside the tube, for instance, mimicking the blood–brain barrier (ECs and astrocytes) or replicating the microvasculature in muscles or other organs. Therefore, rolled-up porous tubes are a next-generation structure useful as cell scaffolds for biological barrier formation and for lab-in-a-tube application.

Acknowledgements

We thank the BIOTEC/CRTD Light Imaging Facility for excellent support with confocal microscopy. The research has received funding from the European Research Council under the European Union's Seventh Framework Programme (FP7/2007-2013)/ERC grant agreement 311529 and the Volkswagen Foundation (no. 86 362).

References

1 T. Kadohama, N. Akasaka, K. Nishimura, Y. Hoshino, T. Sasajima and B. E. Sumpio, *Endothelium: Journal of Endothelial Cell Research*, 2006, **13**, 43–50.
2 G. M. Riha, P. H. Lin, A. B. Lumsden, Q. Z. Yao and C. Y. Chen, *Ann. Biomed. Eng.*, 2005, **33**, 772–779.
3 R. M. Nerem, R. W. Alexander, D. C. Chappell, R. M. Medford, S. E. Varner and W. R. Taylor, *Am. J. Med. Sci.*, 1998, **316**, 169–175.
4 A. B. Fisher, S. Chien, A. I. Barakat and R. M. Nerem, *Am. J. Physiol.: Lung Cell. Mol. Physiol.*, 2001, **281**, L529–L533.
5 L. Cucullo, M. Hossain, V. Puvenna, N. Marchi and D. Janigro, *BMC Neurosci.*, 2011, 12.

Open Access Article. Published on 18 May 2015. Downloaded on 7/17/2025 8:03:40 PM.
This article is licensed under a Creative Commons Attribution-NonCommercial 3.0 Unported Licence.

6 O. C. Colgan, G. Ferguson, N. T. Collins, R. P. Murphy, G. Meade, P. A. Cahill and P. M. Cummins, *Am. J. Physiol.: Heart Circ. Physiol.*, 2007, **292**, H3190–H3197.
7 E. Warabi, Y. Wada, H. Kajiwara, M. Kobayashi, N. Koshiba, T. Hisada, M. Shibata, J. Ando, M. Tsuchiya, T. Kodama and N. Noguchi, *Free Radical Biol. Med.*, 2004, **37**, 682–694.
8 J. M. Tarbell, *Cardiovasc. Res.*, 2010, **87**, 320–330.
9 W. M. Weaver, S. Dharmaraja, V. Milisavljevic and D. Di Carlo, *Lab Chip*, 2011, **11**, 883–889.
10 R. Booth and H. Kim, *Lab Chip*, 2012, **12**, 1784–1792.
11 J. T. Borenstein, M. M. Tupper, P. J. Mack, E. J. Weinberg, A. S. Khalil, J. Hsiao and G. Garcia-Cardena, *Biomed. Microdevices*, 2010, **12**, 71–79.
12 N. J. Douville, Y. C. Tung, R. Li, J. D. Wang, M. E. H. El-Sayed and S. Takayama, *Anal. Chem.*, 2010, **82**, 2505–2511.
13 Z. C. Huang, X. Li, M. Martins-Green and Y. X. Liu, *Biomed. Microdevices*, 2012, **14**, 873–883.
14 S. Kruss, L. Erpenbeck, M. P. Schon and J. P. Spatz, *Lab Chip*, 2012, **12**, 3285–3289.
15 S. H. Ma, L. A. Lepak, R. J. Hussain, W. Shain and M. L. Shuler, *Lab Chip*, 2005, **5**, 74–85.
16 B. Prabhakarpandian, M. C. Shen, J. B. Nichols, I. R. Mills, M. Sidoryk-Wegrzynowicz, M. Aschner and K. Pant, *Lab Chip*, 2013, **13**, 1093–1101.
17 S. Srigunapalan, C. Lam, A. R. Wheeler and C. A. Simmons, *Biomicrofluidics*, 2011, 5.
18 P. A. Vogel, S. T. Halpin, R. S. Martin and D. M. Spence, *Anal. Chem.*, 2011, **83**, 4296–4301.
19 J. H. Yeon, D. Na, K. Choi, S. W. Ryu, C. Choi and J. K. Park, *Biomed. Microdevices*, 2012, **14**, 1141–1148.
20 E. Cukierman, R. Pankov and K. M. Yamada, *Curr. Opin. Cell Biol.*, 2002, **14**, 633–639.
21 Y. Ling, J. Rubin, Y. Deng, C. Huang, U. Demirci, J. M. Karp and A. Khademhosseini, *Lab Chip*, 2007, **7**, 756–762.
22 H. Zhang, S. Dai, J. X. Bi and K. K. Liu, *Interface Focus*, 2011, **1**, 792–803.
23 K. E. Sung, X. J. Su, E. Berthier, C. Pehlke, A. Friedl and D. J. Beebe, *PLoS One*, 2013, 8.
24 P. Zorlutuna, N. Annabi, G. Camci-Unal, M. Nikkhah, J. M. Cha, J. W. Nichol, A. Manbachi, H. J. Bae, S. C. Chen and A. Khademhosseini, *Adv. Mater.*, 2012, **24**, 1782–1804.
25 Y. Hayashi, M. Nomura, S. I. Yamagishi, S. I. Harada, J. Yamashita and H. Yamamoto, *Glia*, 1997, **19**, 13–26.
26 L. L. Bischel, E. W. K. Young, B. R. Mader and D. J. Beebe, *Biomaterials*, 2013, **34**, 1471–1477.
27 M. De Ville, P. Coquet, P. Brunet and R. Boukherroub, *Microfluid. Nanofluid.*, 2012, **12**, 953–961.
28 M. Jamal, S. S. Kadam, R. Xiao, F. Jivan, T. M. Onn, R. Fernandes, T. D. Nguyen and D. H. Gracias, *Adv. Healthcare Mater.*, 2013, **2**, 1142–1150.
29 S. Kim, H. Lee, M. Chung and N. L. Jeon, *Lab Chip*, 2013, **13**, 1489–1500.
30 I. K. Zervantonakis, S. K. Hughes-Alford, J. L. Charest, J. S. Condeelis, F. B. Gertler and R. D. Kamm, *Proc. Natl. Acad. Sci. U. S. A.*, 2012, **109**, 13515–13520.
31 H. Geckil, F. Xu, X. H. Zhang, S. Moon and U. Demirci, *Nanomedicine*, 2010, **5**, 469–484.
32 B. Yuan, Y. Jin, Y. Sun, D. Wang, J. S. Sun, Z. Wang, W. Zhang and X. Y. Jiang, *Adv. Mater.*, 2012, **24**, 890–896.
33 V. Y. Prinz, V. A. Seleznev, A. K. Gutakovsky, A. V. Chehovskiy, V. V. Preobrazhenskii, M. A. Putyato and T. A. Gavrilova, *Phys. E*, 2000, **6**, 828–831.
34 O. G. Schmidt and K. Eberl, *Nature*, 2001, **410**, 168–168.
35 Y. F. Mei, G. S. Huang, A. A. Solovev, E. B. Urena, I. Moench, F. Ding, T. Reindl, R. K. Y. Fu, P. K. Chu and O. G. Schmidt, *Adv. Mater.*, 2008, **20**, 4085–4090.
36 G. S. Huang, Y. F. Mei, D. J. Thurmer, E. Coric and O. G. Schmidt, *Lab Chip*, 2009, **9**, 263–268.
37 E. J. Smith, W. Xi, D. Makarov, I. Monch, S. Harazim, V. A. B. Quinones, C. K. Schmidt, Y. F. Mei, S. Sanchez and O. G. Schmidt, *Lab Chip*, 2012, **12**, 1917–1931.
38 S. Schulze, G. S. Huang, M. Krause, D. Aubyn, V. A. B. Quinones, C. K. Schmidt, Y. F. Mei and O. G. Schmidt, *Adv. Eng. Mater.*, 2010, **12**, B558–B564.
39 W. Xi, C. K. Schmidt, S. Sanchez, D. H. Gracias, R. E. Carazo-Salas, S. P. Jackson and O. G. Schmidt, *Nano Lett.*, 2014, **14**, 4197–4204.
40 C. S. Bausch, A. Koitmae, E. Stava, D. Diedrich, A. Price, P. J. Resto, D. Sonnenberg, C. Heyn, W. Justin, E. Dent and R. H. Blick, *Biophys. J.*, 2013, **104**, 329a–329a.
41 P. Froeter, Y. Huang, O. V. Cangellaris, W. Huang, E. W. Dent, M. U. Gillette, J. C. Williams and X. L. Li, *ACS Nano*, 2014, **8**, 11108–11117.
42 M. R. Yu, Y. Huang, J. Ballweg, H. Shin, M. H. Huang, D. E. Savage, M. G. Lagally, E. W. Dent, R. H. Blick and J. C. Williams, *ACS Nano*, 2011, **5**, 2447–2457.
43 B. Koch, S. Sanchez, C. K. Schmidt, A. Swiersy, S. P. Jackson and O. G. Schmidt, *Adv. Healthcare Mater.*, 2014, **3**, 1753–1758.
44 M. Jamal, N. Bassik, J. H. Cho, C. L. Randall and D. H. Gracias, *Biomaterials*, 2010, **31**, 1683–1690.
45 S. M. Harazim, V. A. B. Quinones, S. Kiravittaya, S. Sanchez and O. G. Schmidt, *Lab Chip*, 2012, **12**, 2649–2655.
46 C. S. Martinez-Cisneros, S. Sanchez, W. Xi and O. G. Schmidt, *Nano Lett.*, 2014, **14**, 2219–2224.
47 C. Heckman, S. Kanagasundaram, M. Cayer and J. Paige, Preparation of cultured cells for scanning electron microscope, *Protoc. Exch.*, 2007, DOI: 10.1038/nprot.2007.504.
48 A. Alajati, A. M. Laib, H. Weber, A. M. Boos, A. Bartol, K. Ikenberg, T. Korff, H. Zentgraf, C. Obodozie, R. Graeser, S. Christian, G. Finkenzeller, G. B. Stark, M. Heroult and H. G. Augustin, *Nat. Methods*, 2008, **5**, 439–445.
49 S. Brouillet, P. Hoffmann, M. Benharouga, A. Salomon, J. P. Schaal, J. J. Feige and N. Alfaidy, *Mol. Biol. Cell*, 2010, **21**, 2832–2843.
50 S. K. Kang, S. W. Hwang, H. Y. Cheng, S. Yu, B. H. Kim, J. H. Kim, Y. G. Huang and J. A. Rogers, *Adv. Funct. Mater.*, 2014, **24**, 4427–4434.
51 T. Chappex and K. L. Scrivener, *Cem. Concr. Res.*, 2012, **42**, 1645–1649.
52 E. Kang, S. J. Shin, K. H. Lee and S. H. Lee, *Lab Chip*, 2010, **10**, 1856–1861.

 This journal is © The Royal Society of Chemistry 2015

Open Access Article. Published on 18 May 2015. Downloaded on 7/17/2025 8:03:40 PM.
This article is licensed under a Creative Commons Attribution-NonCommercial 3.0 Unported Licence.

53 L. M. Li, X. Y. Wang, L. S. Hu, R. S. Chen, Y. Huang, S. J. Chen, W. H. Huang, K. F. Huo and P. K. Chu, *Lab Chip*, 2012, **12**, 4249–4256.
54 S. Zakharchenko, N. Puretskiy, G. Stoychev, C. Waurisch, S. G. Hickey, A. Eychmuller, J. U. Sommer and L. Ionov, *J. Mater. Chem. B*, 2013, **1**, 1786–1793.
55 A. R. Butler and D. L. H. Williams, *Chem. Soc. Rev.*, 1993, **22**, 233–241.
56 J. P. Cooke and V. J. Dzau, *Annu. Rev. Med.*, 1997, **48**, 489–509.
57 J. M. Mclenachan, J. Vita, R. D. Fish, C. B. Treasure, D. A. Cox, P. Ganz and A. P. Selwyn, *Circulation*, 1990, **82**, 1169–1173.
58 K. Malachowski, M. Jamal, Q. R. Jin, B. Polat, C. J. Morris and D. H. Gracias, *Nano Lett.*, 2014, **14**, 4164–4170.
59 V. Linder, B. D. Gates, D. Ryan, B. A. Parviz and G. M. Whitesides, *Small*, 2005, **1**, 730–736.
60 M. B. Esch, G. J. Mahler, T. Stokor and M. L. Shuler, *Lab Chip*, 2014, **14**, 3081–3092.
61 J. B. Lee and J. H. Sung, *Biotechnol. J.*, 2013, **8**, 1258–1266.
62 M. L. Shuler and M. Esch, *J. Tissue Eng. Regener. Med.*, 2012, **6**, 347–347.
63 A. Williamson, S. Singh, U. Fernekorn and A. Schober, *Lab Chip*, 2013, **13**, 3471–3480.